ACS APPLIED MATERIALS & INTERFACES

Research Article

www.acsami.org

Double-Phase-Functionalized Magnetic Janus Polymer Microparticles Containing TiO_2 and Fe_2O_3 Nanoparticles Encapsulated in Mussel-Inspired Amphiphilic Polymers

Hiroshi Yabu,*[,†,‡] Hiroyuki Ohshima,[†] and Yuta Saito[†]

[†]Institute of Multidisciplinary Research for Advanced Materials (IMRAM), Tohoku University, 2-1-1 Katahira, Aoba-Ku, Sendai, Tōhoku, 980-8577, Japan

[‡]Precursory Research for Embryonic Science and Technology (PRESTO), Japan Science and Technology Agency (JST), 4-1-8 Honcho, Kawaguchi, Saitama 332-0012, Japan

Supporting Information

ABSTRACT: Recently, anisotropic colloidal polymeric materials including Janus microparticles, which have two distinct aspects on their surfaces or interiors, have garnered much interest due to their anisotropic alignment and rotational orientation with respect to external electric or magnetic fields. Janus microparticles are also good candidates for pigments in "twisting ball type" electronic paper, which is considered promising for next-generation flexible display devices. We demonstrate here a universal strategy to encapsulate inorganic nanoparticles and to introduce different such inorganic nanoparticles into distinct polymer phases in Janus microparticles. TiO_2 and Fe_2O_3 nanoparticles were separately encapsulated in two different mussel-inspired amphiphilic copolymers, and then organic−inorganic composite Janus microparticles were prepared by simple evaporation of solvent from the dispersion containing the polymer and nanoparticle. These Janus microparticles were observed to rotate quickly in response to applied magnetic fields.

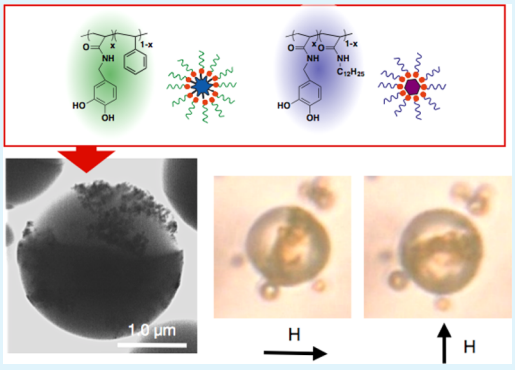

KEYWORDS: *Janus particles, inorganic nanoparticles, mussel-inspired, amphiphilic polymers, phase separation*

1. INTRODUCTION

Recently, anisotropic colloidal polymeric materials including Janus microparticles, which have two distinct aspects on their surfaces or interiors, have attracted increased interest because of their anisotropic alignment and rotational orientation with respect to external electric or magnetic fields.[1−5] Such alignment and orientation can be controlled by adjusting the electronic and magnetic properties in each aspect of a Janus particle. The unique electronic, magnetic and interfacial properties of Janus particles have been investigated,[6−8] and they are also good candidates for pigments in twisting ball type electronic paper, which is considered promising for next-generation flexible display devices.[9] Furthermore, a wide variety of applications of Janus particles that respond to external electronic and magnetic fields have been reported, such as magnetically induced locomotion,[10,11] formation of unique assemblies,[6,12−14] and stabilization of liquid−liquid interfaces.[13,15] To apply Janus microparticles as pigments in electronic paper, the size and color of each phase as well as the response to external fields should be optimized to achieve high-resolution, multicolored, and quick-response electronic paper.[16,17]

Several methods for fabricating Janus microparticles have been reported, including evaporation of solvent from emulsions containing two distinct polymers,[18] seed polymerization,[19] and evaporation of metals onto embedded polymer particles.[20] Block copolymers have also been used as precursors of Janus nanoparticles.[21] Other techniques for the preparation of Janus particles are well described in recent review papers.[1,22] Recently, we developed a novel method, termed self-organized precipitation (SORP), to fabricate submicrometer-sized polymer-containing Janus particles by simple evaporation of a good solvent from a polymer blend solution containing a poor solvent.[23,24] When using SORP, interior structures of polymer-containing microparticles can be controlled by the phase separation of blended polymers from a core−shell to Janus-type structure. This separation is brought about by changing the combinations of polymers according to the Flory−Huggins solubility parameters of the blended polymers.[25] In the case of polystyrene (PS) and polyisoprene (PI), Janus-structured microparticles have been successfully fabricated.[26] Furthermore, magnetic Janus particles containing magnetic nanoparticles have also been fabricated whose surfaces were encapsulated in amphiphilic block copolymers or surface-initiated hydrophobic

Received: July 28, 2014
Accepted: September 29, 2014
Published: September 29, 2014

Scheme 1. Chemical structures of polymers used in this experiment

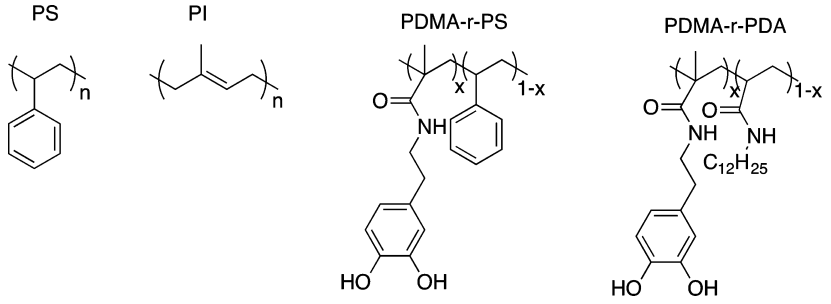

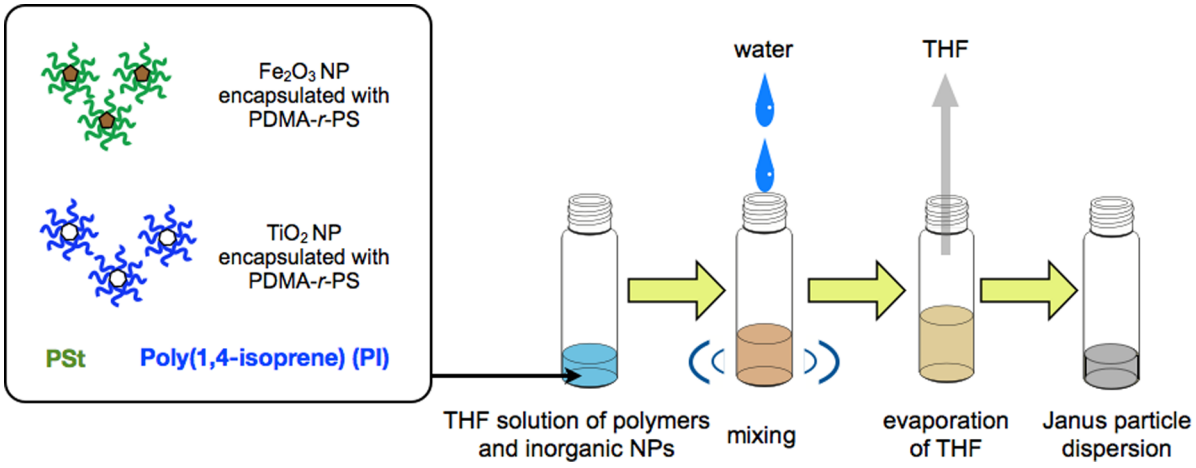

Figure 1. Schematic illustration of Janus particle preparation.

polymer brushes with high affinity to the PS phase.[27,28] However, only a single phase of the Janus microsphere was colored and functionalized.

To functionalize both phases of Janus microparticles with functional inorganic nanoparticles, a universal strategy for stabilizing these functional nanomaterials with arbitrary hydrophobic polymers is required. Amphiphilic polymers have generally been used for stabilizing inorganic nanoparticles.[29,30] However, the affinity of amphiphilic polymers for inorganic nanoparticles strongly depends on specific interactions between hydrophilic groups of amphiphilic polymers and the inorganic nanoparticles. It is therefore still challenging to encapsulate a wide variety of inorganic nanoparticles in amphiphilic polymers having arbitrary hydrophobic blocks.

Catechol groups, which are present in the adhesive proteins of mussels, show excellent adhesion properties for a wide variety of materials including noble metals, metal oxides, ceramics, and even on polytetrafluoroethyrene (PTFE).[31−33] Polydopamine has been used as an adhesive layer for metals and polymers due to its molecular-scale flatness that can align hydroxyl groups; such alignment is in general strongly related to adhesion properties.[34−36] Many reports have described the adhesion of certain synthetic polymers or polypeptides, those that contain catechol groups at the ends of the main chains or on the side chains, to the surfaces of various materials. In those reports, catechol moieties adhere to bulk metals or metal oxides by chelation and coordination, especially in the case of iron oxide, and hydrophilicity and hydrogen bonding support their adhesion.[37−40] Anchoring amphiphilic molecules containing catechol moieties onto inorganic nanoparticles was shown to allow the dispersion of the inorganic nanoparticles into organic solvents.[33] We have recently reported that Al_2O_3 nanoparticles can be encapsulated in amphiphilic copolymers containing catechol moieties as side chains in organic solvents.[41] Polymers containing catechol groups as side chains strongly adhere to glass, aluminum, and even PTFE, and these polymers have been utilized as an adhesive for sticking porous materials onto various substrates[42] and as adhesion layers between polymer resins and substrates in thermal nanoimprint lithography.[43]

Here, we demonstrate a universal strategy to encapsulate inorganic nanoparticles so that different inorganic nanoparticles can be introduced into distinct polymer phases in Janus microparticles. Two different mussel-inspired amphiphilic copolymers containing catechol groups as side chains and containing different hydrophobic groups were synthesized. TiO_2 and Fe_2O_3 nanoparticles were separately encapsulated in these two copolymers, and then organic−inorganic composite Janus microparticles were prepared by SORP. Characterization of their interior structures and their responses to externally applied magnetic fields are discussed.

2. EXPERIMENTAL SECTION

Scheme 1 shows the chemical structures of the synthesized polymers. Polystyrene (PS, MW = 13.2 kg/mol) and 1,4-polyisoprene (PI, MW = 35 kg/mol) were purchased from Polymer Source Inc. The detailed synthetic routes of the mussel-inspired amphiphilic copolymers (polydimethylacrylamide (PDMA)-*r*-PS and PDMA-*r*-PDA) are shown in the electric Supporting Information. The monomers and amphiphilic copolymers were synthesized as previously reported, with minor modification.[42]

Titanium(IV) dioxide (TiO_2) nanoparticles (average diameter = 21 nm, 99.5% pure) and γ-Fe_2O_3 nanoparticles (average diameter = 20−30 nm, 98% pure) were purchased from Sigma-Aldrich (Japan) and Nanostructured & Amorphous Materials Inc., respectively. TiO_2 nanoparticles were dispersed in THF using ultrasonication, and then

5 mL of PDMA-*r*-PDA (10 mg/mL) was added into the solution. After 5 min of the sonication, the dispersion was shaken for 12 h. PDMA-*r*-PDA-encapsulated TiO_2 nanoparticles were collected by centrifugation (10,000 rpm, 15 min, 5 °C) and then redispersed in THF. This process was repeated three times to remove excess PDMA-*r*-PDA. Finally, the collected PDMA-*r*-PDA-encapsulated TiO_2 nanoparticles were dried in vacuo. The same procedures were performed to prepare Fe_2O_3 nanoparticles encapsulated with PDMA-*r*-PS, except that the Fe_2O_3 nanoparticles were collected by using a neodymium magnet instead of ultracentrifugation. Sizes of polymer-encapsulated nanoparticles were measured by dynamic light scattering (DLS) (Zetasizer Nano ZS, Malvern). Fourier-transform infrared (FT-IR) spectroscopy was performed by preparing KBr pellets containing sample specimen (FT-6000, Jasco).

Figure 1 shows a schematic illustration of the preparation of Janus microparticles. A one-to-one mixture of THF solutions of PS (1.0 mg/mL) and PI (1.0 mg/mL) was prepared. Then, 100 μL of PDMA-*r*-PDA-encapsulated TiO_2 nanoparticles (1.0 mg/mL), 100 μL of PDMA-*r*-PS-encapsulated Fe_2O_3 nanoparticles (1.0 mg/mL), and 100 μL of both nanoparticles were respectively added into three separate 1 mL samples of the PS−PI solution in THF. After addition of 1 mL of membrane-filtered water (Milli-Q, Millipore), the solutions were left uncovered for 2 days, allowing the THF to evaporate. Finally, the composite particles were obtained.

Sizes of composite particles were measured by DLS. To observe the surface and interior structures of the composite particles, scanning electron microscopy (SEM, S-5200, Hitachi Japan), scanning transmission electron microscopy (STEM, S-5200 equipped with an STEM unit, Hitachi) and transmission electron microscopy (TEM, H-7650, Hitachi) were performed. Sample specimens were prepared by casting an aqueous dispersion of the composite particles after staining with aq. 0.2 wt % OsO_4 for 2 h and were collected by ultracentrifugation (10 000 rpm, 15 min, 5 °C) onto a Cu grid with a collodion membrane. Energy dispersive X-ray (EDX) spectroscopy was performed by EDAX Genesis (Ametek).

Aqueous dispersions of the composite particles were cast on a glass coverslip coated with polydimethylsiloxane spacer, and covered with another glass coverslip. The rotational motion of composite particles was evaluated under an optical microscope (VHX-900, Keyence) by moving a neodymium magnet (held 10 cm away from the sample) that produces an applied 1 mT magnetic field on the sample.[28] The rotational motion was captured as video movies and the rotational speed (the amount of time it took to rotate the Janus particles by 90°) were calculated.

3. RESULTS AND DISCUSSION

Figure 2a and c shows, respectively, the hydrodynamic diameters (D_h) of PDMA-*r*-PS-encapsulated Fe_2O_3 and PDMA-*r*-PDA-encapsulated TiO_2 nanoparticles dispersed in THF. The hydrodynamic diameters of encapsulated Fe_2O_3 and TiO_2 nanoparticles were measured to be 258 nm (polydispersity index, PDI = 0.29) and 261 nm (PDI = 0.19). Since these values are 10 times larger than the initial sizes of the inorganic nanoparticles, the inorganic nanoparticles underwent secondary aggregation.

Figure 2b and d shows TEM images of PDMA-*r*-PS-encapsulated Fe_2O_3 nanoparticles and PDMA-*r*-PDA-encapsulated TiO_2 nanoparticles, respectively. Some nanoparticles were observed to be aggregated in the TEM images, and the average size of a single aggregation in these images agreed well with the D_h value. Polymer layers fill the gaps between the nanoparticles. Since nanoparticles have high surface free energies, it is difficult to disperse individual nanoparticles by using ultrasonication to break down the large aggregates into small aggregates in THF. These results are the same as those found for other inorganic nanoparticles that we reported previously.

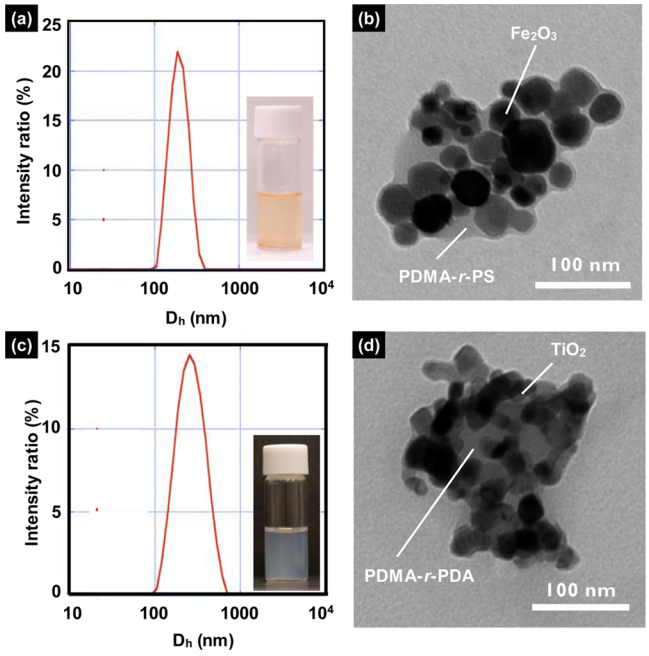

Figure 2. DLS measurements (a and c) and TEM images (b and d) of PDMA-*r*-PS-encapsulated Fe_3O_3 nanoparticles (a and b) and PDMA-*r*-PDA-encapsulated TiO_2 nanoparticles (c and d).

Figure 3a shows FT-IR spectra of Fe_2O_3 nanoparticles, PDMA-*r*-PS-encapsulated Fe_2O_3 nanoparticles, and PDMA-*r*-PS. There is no specific absorption observed for Fe_2O_3 nanoparticles. PS-*r*-PDMA has specific absorption peaks attributed to ν(Ar−O) (a, 1282 cm^{-1}), d(Ar−O) (b, 1368 cm^{-1}), $\delta(CH_2)$ (c, 1452 cm^{-1}), ν(C═C) (d, 1492 cm^{-1} and e, 1600 cm^{-1}), $\nu(C{=}O)_{amide}$ (f, 1680 cm^{-1}), $\nu_s(CH_2)$ (h, 2850 cm^{-1}) and $\nu_{as}(CH_2)$ (i, 2,927 cm^{-1}). Since PDMA-*r*-PS-encapsulated Fe_2O_3 nanoparticles show the same absorption peaks as PDMA-*r*-PS, Fe_2O_3 nanoparticles were covered with PDMA-*r*-PS. The disappearance of the peak at Figure 3a-a may be explained by coordination of catecholic moieties onto Fe_2O_3 nanoparticles.[39] This result also supports a strong adhesion of PDMA-*r*-PS onto Fe_2O_3 nanoparticles.

Figure 3b shows FT-IR spectra of TiO_2 nanoparticles, PDMA-*r*-PDA-encapsulated TiO_2 nanoparticles, and PDMA-*r*-PDA. As in the case of the Fe_2O_3 nanoparticles, there is no specific absorption attributed to TiO_2 nanoparticles (exceptional for a trace of a carbonyl group adhered on the surface of TiO_2 nanoparticles from their synthesis). PDMA-*r*-PDA has specific absorption peaks attributed to ν(Ar−O) (a, 1,282 cm^{-1}), d(Ar−O) (b, 1,368 cm^{-1}), $\delta(CH_2)$ (c, 1,468 cm^{-1}), $\nu(N{-}H)_{amide}$ (d, 1,552 cm^{-1}), $\nu(C{=}O)_{amide}$ (e, 1,680 cm^{-1}), $\nu_s(CH_2)$ (f, 2,861 cm^{-1}), and $\nu_{as}(CH_2)$ (g, 2,936 cm^{-1}), and these peaks were clearly observed for PDMA-*r*-PDA-encapsulated TiO_2 nanoparticles. These results imply that TiO_2 nanoparticles were covered with PDMA-*r*-PDA.

Figure 4 shows the relative stabilities of the different particles dispersed in THF. Soon after the Fe_2O_3 nanoparticles and PS-*r*-PDMA-encapsulated Fe_2O_3 nanoparticles were subjected to ultrasonication, both of them were indeed observed to be dispersed in the THF solution (Figure 4a). After standing for 1 day, however, unencapsulated Fe_2O_3 nanoparticles completely precipitated, whereas PDMA-*r*-PS-encapsulated Fe_2O_3 nanoparticles remained dispersed in the THF solution (Figure 4b).

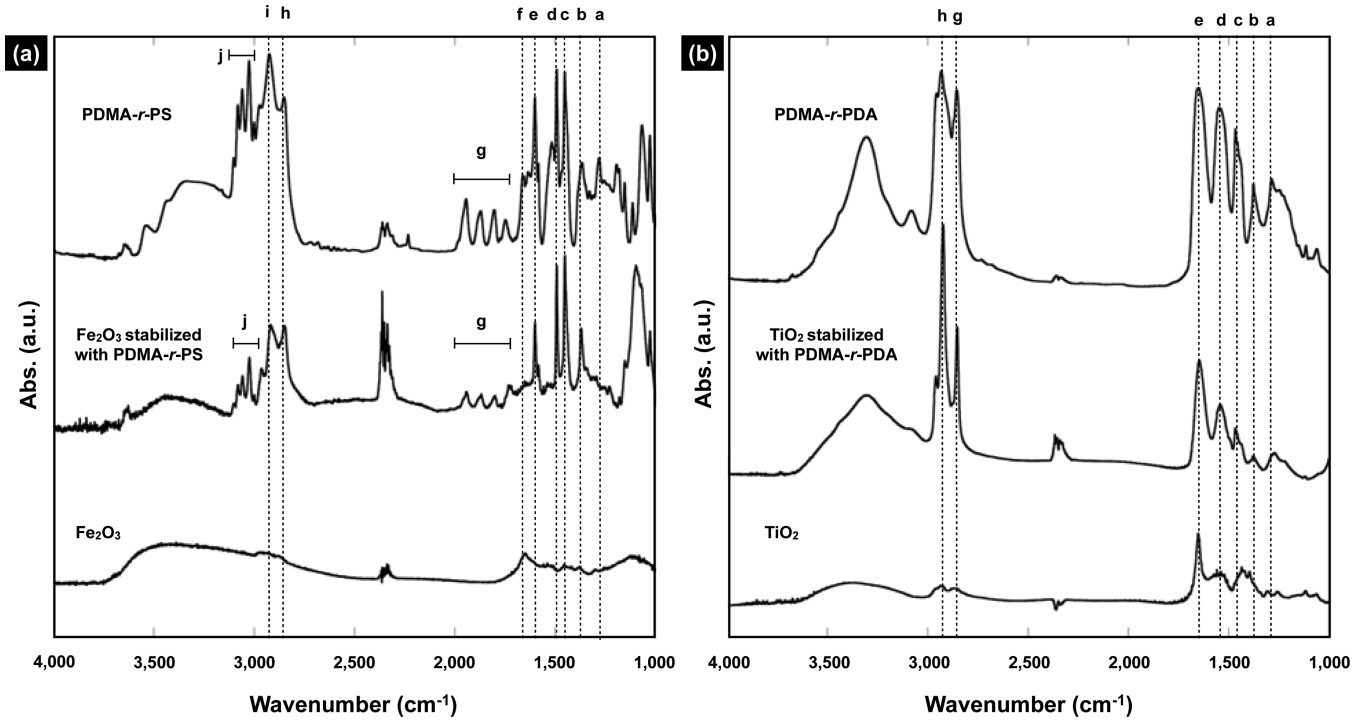

Figure 3. FT-IR spectra of Fe_3O_3 nanoparticles, PDMA-*r*-PS-encapsulated Fe_3O_3 nanoparticles, and PDMA-*r*-PS (a), as well as of TiO_2 nanoparticles, PDMA-*r*-PDA-encapsulated TiO_2 nanoparticles, and PDMA-*r*-PDA (b).

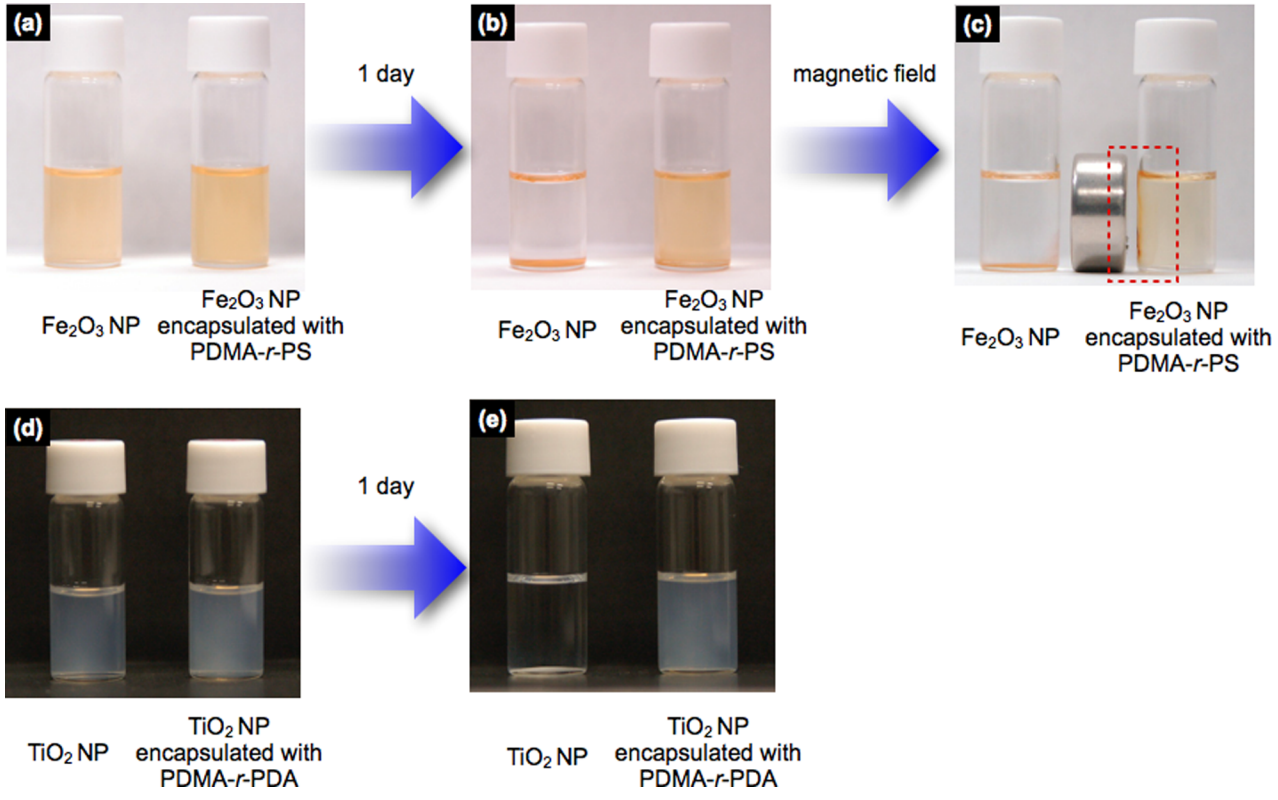

Figure 4. Visual evaluation of the stabilities of the inorganic nanoparticles (Fe_2O_3 (a, b), TiO_2 (d, e)) with and without encapsulation. Magnetic response of dispersed Fe_2O_3 nanoparticles was also evaluated (c).

Moreover, the dispersed PDMA-*r*-PS-encapsulated Fe_2O_3 nanoparticles were observed to congregate near a magnet (Figure 4c). In contrast, the extensively aggregated and sedimented bare Fe_2O_3 nanoparticles at the bottom of the glass bottle did not respond to the magnet. These particles did not have enough mobility to overcome the aggregated and sedimented state to respond to the magnetic field, likely because the magnetization of Fe_2O_3 nanoparticles is, as is well-

dx.doi.org/10.1021/am506530s | ACS Appl. Mater. Interfaces 2014, 6, 18122−18128

known, not very strong. These results show that PDMA-*r*-PS-encapsulated Fe_2O_3 nanoparticles have high solubility in THF and can maintain its magnetic properties over time. TiO_2 nanoparticles encapsulated in PDMA-*r*-PDA also showed good stability in THF (Figures 4d and 4e).

Taken together, these observations indicate that encapsulation in the tested amphiphilic polymers stabilized the dispersions of the inorganic particles in THF. Moreover, note that due to the high adhesion properties of catechol moieties with the inorganic nanoparticles, the catechol-containing amphiphilic polymers make the resulting encapsulated nanoparticles more stable in a mixture of hydrophobic organic solvent and water than do other amphiphilic polymers that contain carboxylic acid, which is usually used as the hydrophilic group in amphiphilic molecules (see Supporting Information, S6).

To confirm the selective introduction of Fe_2O_3 nanoparticles and TiO_2 nanoparticles encapsulated in the different mussel-inspired amphiphilic copolymers, microparticles comprised of PS, PI, and inorganic nanoparticles were prepared by using SORP.

Figure 5a and b, respectively, shows STEM and cross-sectional TEM images of a microparticle consisting of PS, PI,

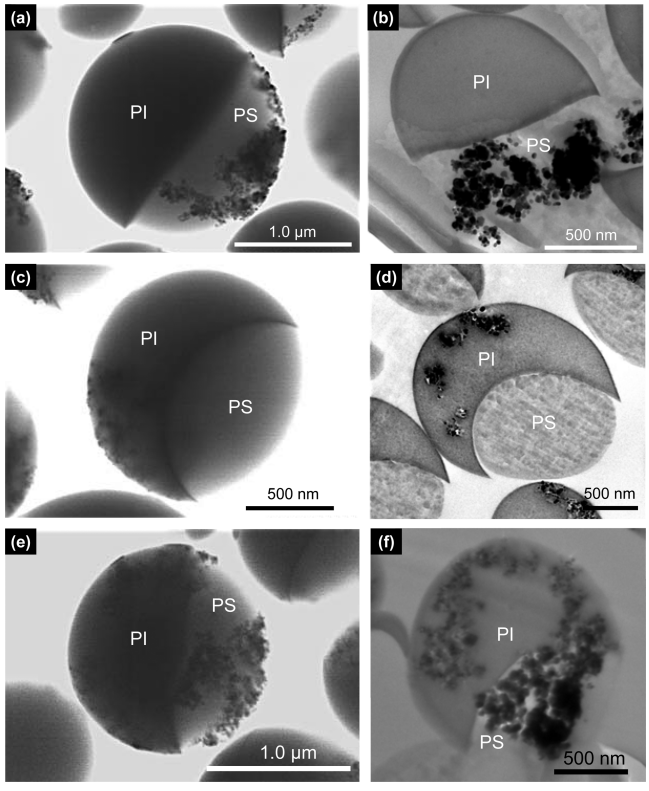

Figure 5. STEM images (a, c, e) and cross-sectional TEM images (b, d, f) of Janus particles containing PDMA-*r*-PS-encapsulated Fe_3O_3 nanoparticles (a, b), Janus particles containing PDMA-*r*-PDA-encapsulated TiO_2 nanoparticles (c, d), and double-phase-functionalized Janus particles (e, f).

and PDMA-*r*-PS-encapsulated Fe_2O_3 nanoparticles. Janus-type phase-separated structures consisting of a dark gray PI phase, which was stained with OsO_4, and a light gray PS phase, were clearly imaged. Furthermore, black dots attributed to Fe_2O_3 nanoparticles were also imaged, in only the PS phase. From the cross-sectional TEM image, Janus-type phase separation and introduction of Fe_2O_3 nanoparticles were also observed in the microparticles.

In contrast, TiO_2 nanoparticles were located in only the PI phase when the microparticles were prepared from PS, PI and PDA-*r*-PDMA encapsulated TiO_2 nanoparticles (Figure 5c and 5d). These differences originated from the difference of the copolymerized monomers of PDMA, that is, PS and PDA, which have high affinities for the PS and PI phases, respectively. While PDMA is adhered on the surface of the TiO_2 nanoparticles, side chain alkyl groups of PDA of PDA-*r*-PDMA are located on the surface of encapsulated TiO_2 nanoparticles. Alkyl groups have higher affinity for hydrocarbons including polyisoprene than for aromatic polystyrene. On the other hand, PDMA-*r*-PS has PS moieties, and the Fe_2O_3 nanoparticles have high affinity for the PS hemisphere. As the result, selective introduction of nanoparticles was controlled by changing the surface-encapsulating polymers.

By using the phase selectivity of mussel-inspired amphiphilic copolymer-encapsulated inorganic nanoparticles, single-phase- and double-phase-functionalized Janus particles can be prepared. Microparticles consisting of PS, PI, PDMA-*r*-PS-encapsulated Fe_2O_3 nanoparticles and PDMA-*r*-PDA-encapsulated TiO_2 nanoparticles were prepared from their THF solution by SORP with water used as a poor solvent. From DLS measurement, the average size of these prepared microparticles was observed to be 880 nm. Figure 5e and 5f, respectively, show STEM and cross-sectional TEM images of these prepared microparticles. In both images, Janus-type phase separation was observed and inorganic nanoparticles shown as black dots were introduced into both phases. The average diameter of the Janus particles was 740 ± 120 nm (PDI = 0.096). Low magnification cross-sectional TEM images reveal that inorganic nanoparticles were introduced as grains in each polymer phase, reflecting their secondary aggregation structures.

Figure 6 shows a composite image of a cross-sectional TEM image and energy-dispersive X-ray spectroscopy mapping of Janus microspheres containing two distinct types of inorganic nanoparticles. From the composite image, signals for Fe (blue) were observed to be located at the unstained PS phase, and signals for Ti (pink) were observed to be located at the PI phase, which was stained with OsO_4 (Os, yellow).These results

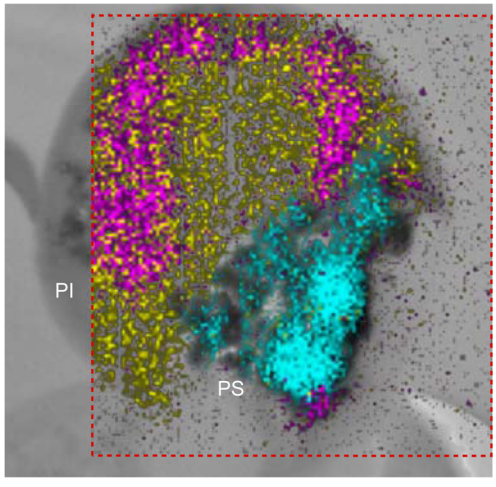

Figure 6. Superimposed image of energy-dispersive X-ray spectroscopy mapping of Ti−K (pink), Os−M (yellow), and Fe−K (blue) onto a cross-sectional TEM image.

dx.doi.org/10.1021/am506530s | *ACS Appl. Mater. Interfaces* 2014, 6, 18122−18128

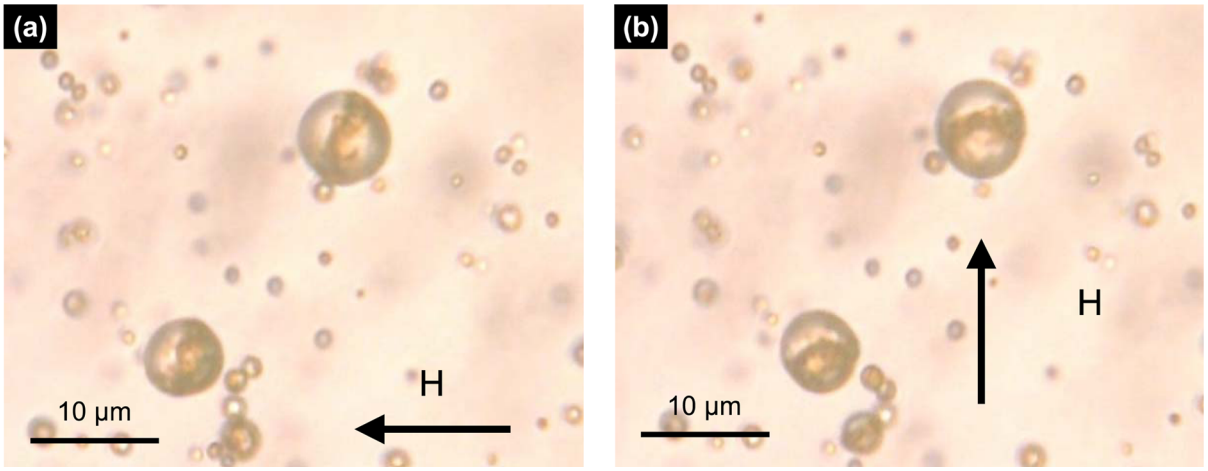

Figure 7. Horizontal (a) and vertical (b) alignments of double-phase-functionalized Janus particles along the cell planes in response to magnetic fields.

show that double-phase-functionalized Janus particles containing functional nanoparticles such as Fe_2O_3 and TiO_2 nanoparticles were successfully prepared.

To see how the double-phase-functionalized Janus microparticles react to applied magnetic fields, an aqueous dispersion of these microparticles was injected in a glass cell prepared on a glass slip, and then the alignments of the microparticles in response to a neodymium magnet were observed under an optical microscope. Figures 7a and 7b show different alignments of Janus microparticles along the applied magnetic fields. For ease of observation, we chose large Janus particles (~7 μm) to check the rotational motion in response to the magnetic field. Since Janus microparticles were colored white in the TiO_2 phase and brown in the Fe_2O_3 phases, the Janus-type phase-separated structure was clearly imaged by using the optical microscope.

The alignment experiment also showed the course of the rotation of the Janus microparticles in response to the magnetic fields. Note that Janus particles accumulate due to magnetic dipole−dipole interactions upon application of a strong magnetic field (more than about 50 mT),[44] but only a moderate magnetic field (~1 mT) was required to rotate the Janus microparticles. We observed that the microparticles reacted to the magnetic field within a few hundreds of milliseconds in water (see video in the Supporting Information), which is at least as fast as the response time of existing electrophoretic electric paper.[45] Note that double-phase-functionalized Janus particles show high scattering due to the high refractive index of TiO_2 nanoparticles (see Supporting Information, S7). In contrast to the single-phase-functionalized Janus particles, the high contrast between the PI phase containing TiO_2 nanoparticles and the PS phase containing Fe_2O_3 in the double-phase-functionalized Janus particles makes these particles suitable for use as pigments in electronic paper.

4. CONCLUSION

We succeeded in fabricating double-phase-functionalized composite Janus particles by the SORP method and using inorganic nanoparticles encapsulated in mussel-inspired amphiphilic copolymers. This strategy paves the way for the fabrication of Janus particles having various kinds of functional inorganic nanoparticles included in the specific phases. Furthermore, the use of amphiphilic copolymers shown in this report provides a simple approach for creating polymer-encapsulated inorganic nanoparticles. The double-phase-functionalized Janus particles are promising for use not only as pigments in electronic paper, but also as as immunoassay probes,[46] nanoscale valves,[47] and a variety of other applications.[21,48−50]

■ ASSOCIATED CONTENT

Ⓢ Supporting Information

Synthetic methods for the mussel-inspired amphiphilic copolymers and a movie of the magnetic Janus particles rotating in response to applied magnetic fields. This material is available free of charge via the Internet at http://pubs.acs.org/.

■ AUTHOR INFORMATION

Corresponding Author

*E-mail: yabu@tagen.tohoku.ac.jp.

Author Contributions

H.Y. conceived and designed the experiments. Y.S. and H.O. performed the experiments. H.Y. and Y.S. collected the data. H.Y. wrote the manuscript.

Funding

This research has partially been supported by Grant-in-Aid for Young Researchers (A) (No. 26708025), JSPS, Japan.

Notes

The authors declare no competing financial interest.

■ ACKNOWLEDGMENTS

Authors thank Ms. Minori Suzuki for helping cross-sectional TEM observations.

■ REFERENCES

(1) Walther, A.; Müller, A. H. E. *Chem. Rev.* **2013**, *113*, 5194−5261.
(2) Dendukuri, D.; Pregibon, D.; Collins, J.; Hatton, T.; Doyle, P. *Nat. Mater.* **2006**, *5*, 365−369.
(3) Xie, H.; She, Z.-G.; Wang, S.; Sharma, G.; Smith, J. W. *Langmuir* **2012**, *28*, 4459−4463.
(4) Wurm, F.; Kilbinger, A. F. M. *Angew. Chem., Int. Ed.* **2009**, *48*, 8412−8421.
(5) Lin, C.-C.; Liao, C.-W.; Chao, Y.-C.; Kuo, C. *ACS Appl. Mater. Interfaces* **2010**, *2*, 3185−3191.
(6) Ruditskiy, A.; Ren, B.; Kretzschmar, I. *Soft Matter* **2013**, *9*, 9174−9181.

(7) Rezvantalab, H.; Shojaei-Zadeh, S. *Soft Matter* **2013**, *9*, 3640−3650.
(8) Moghani, M. M.; Khomami, B. *Soft Matter* **2013**, *9*, 4815−4821.
(9) Nisisako, T.; Torii, T.; Takahashi, T.; Takizawa, Y. *Adv. Mater.* **2006**, *18*, 1152.
(10) Baraban, L.; Makarov, D.; Schmidt, O. G.; Cuniberti, G.; Leiderer, P.; Erbe, A. *Nanoscale* **2013**, *5*, 1332.
(11) Baraban, L.; Streubel, R.; Makarov, D.; Han, L.; Karnaushenko, D.; Schmidt, O. G.; Cuniberti, G. *ACS Nano* **2013**, *7*, 1360−1367.
(12) Brugarolas, T.; Tu, F.; Lee, D. *Soft Matter* **2013**, *9*, 9046−9058.
(13) Kumar, A.; Park, B. J.; Tu, F.; Lee, D. *Soft Matter* **2013**, *9*, 6604−6617.
(14) Lee, S. Y.; Yang, S. *Angew. Chem., Int. Ed.* **2013**, *52*, 8160−8164.
(15) Fujii, S.; Yokoyama, Y.; Miyanari, Y.; Shiono, T.; Ito, M.; Yusa, S.-I.; Nakamura, Y. *Langmuir* **2013**, *29*, 5457−5465.
(16) Nie, Z.; Li, W.; Seo, M.; Xu, S.; Kumacheva, E. *J. Am. Chem. Soc.* **2006**, *128*, 9408−9412.
(17) Schryen, G.; Karla, J. *Wirtschaftsinf* **2002**, *44*, 567−574.
(18) Tanaka, T.; Nakatsuru, R.; Kagari, Y.; Saito, N.; Okubo, M. *Langmuir* **2008**, *24*, 12267−12271.
(19) Ahmad, H.; Saito, N.; Kagawa, Y.; Okubo, M. *Langmuir* **2008**, *24*, 688−691.
(20) Xia, D.; Johnson, L. M.; López, G. P. *Adv. Mater. Weinheim* **2012**, *24*, 1287−1302.
(21) Lattuada, M.; Hatton, T. A. *Nano Today* **2011**, *6*, 286−308.
(22) Loget, G.; Kuhn, A. *J. Mater. Chem.* **2012**, *22*, 15457.
(23) Yabu, H. *Bull. Chem. Soc. Jpn.* **2012**, *85*, 265−274.
(24) Yabu, H. *Polym. J.* **2012**, *45* (3), 261−268.
(25) Motoyoshi, K.; Tajima, A.; Higuchi, T.; Yabu, H.; Shimomura, M. *Soft Matter* **2010**, *6*, 1253−1257.
(26) Higuchi, T.; Tajima, A.; Yabu, H.; Shimomura, M. *Soft Matter* **2008**, *4*, 1302.
(27) Arita, T.; Kanahara, M.; Motoyoshi, K.; Koike, K.; Higuchi, T.; Yabu, H. *J. Mater. Chem. C* **2012**, *1*, 207−212.
(28) Yabu, H.; Kanahara, M.-A.; Shimomura, M.; Arita, T.; Harano, K.; Nakamura, E.; Higuchi, T.; Jinnai, H. *ACS Appl. Mater. Interfaces* **2013**, *5* (8), 3262−3266.
(29) Du, B.; Zhao, B.; Tao, P.; Yin, K.; Lei, P.; Wang, Q. *Colloids Surf. A* **2008**, *317*, 194−205.
(30) Hickey, R. J.; Haynes, A. S.; Kikkawa, J. M.; Park, S.-J. *J. Am. Chem. Soc.* **2011**, *133*, 1517−1525.
(31) Waite, J. H.; Housley, T. J.; Tanzer, M. L. *Biochemistry* **1985**, *24*, 5010−5014.
(32) Lee, H.; Lee, B. P.; Messersmith, P. B. A. *Nature* **2007**, *448*, 338−341.
(33) Fan, X.; Lin, L.; Dalsin, J. L.; Messersmith, P. B. *J. Am. Chem. Soc.* **2005**, *127*, 15843−15847.
(34) Zangmeister, R. A.; Morris, T. A.; Tarlov, M. J. *Langmuir* **2013**, *29*, 8619−8628.
(35) Wei, Q.; Yu, B.; Wang, X.; Zhou, F. *Macromol. Rapid Commun.* **2014**, *35*, 1046−1054.
(36) Dreyer, D. R.; Miller, D. J.; Freeman, B. D.; Paul, D. R.; Bielawski, C. W. *Langmuir* **2012**, *28*, 6428−6435.
(37) Lee, H.; Lee, B. P.; Messersmith, P. B. *Nature* **2007**, *448*, 338−341.
(38) Westwood, G.; Horton, T. N.; Wilker, J. J. *Macromolecules* **2007**, *40*, 3960−3964.
(39) Zvarec, O.; Purushotham, S.; Masic, A.; Ramanujan, R. V.; Miserez, A. *Langmuir* **2013**, *29*, 10899−10906.
(40) Wei, W.; Yu, J.; Broomell, C.; Israelachvili, J. N.; Waite, J. H. *J. Am. Chem. Soc.* **2013**, *135*, 377−383.
(41) Saito, Y.; Shimomura, M.; Yabu, H. *Chem. Commun.* **2013**, *49*, 6081−6083.
(42) Saito, Y.; Kawano, T.; Shimomura, M.; Yabu, H. *Macromol. Rapid Commun.* **2013**, *34*, 630−634.
(43) Yabu, H.; Saito, Y.; Shimomura, M.; Matsuo, Y. *J. Mater. Chem. C* **2013**, *1*, 1558.
(44) Ren, B.; Ruditskiy, A.; Song, J. H. K.; Kretzschmar, I. *Langmuir* **2012**, *28*, 1149−1156.
(45) Kao, W.-C.; Ye, J.-A.; Lin, F.-S.; Cheng, P.-Y.; Sprague, R. *IEEE Trans.Consumer Electronics* **2009**, *55*, 1−5.
(46) Ueda, E.; Levkin, P. A. *Adv. Mater. Weinheim* **2013**, *25*, 1234−1247.
(47) Daghighi, Y.; Li, D. *Lab Chip* **2011**, *11*, 2929−2940.
(48) Mun, J. H.; Chang, Y. H.; Shin, D. O.; Yoon, J. M.; Choi, D. S.; Lee, K.-M.; Kim, J. Y.; Cha, S. K.; Lee, J. Y.; Jeong, J.-R.; Kim, Y.-H.; Kim, S. O. *Nano Lett.* **2013**, *13*, 5720−5726.
(49) Shin, D. O.; Mun, J. H.; Hwang, G.-T.; Yoon, J. M.; Kim, J. Y.; Yun, J. M.; Yang, Y.-B.; Oh, Y.; Lee, J. Y.; Shin, J.; Lee, K. J.; Park, S.; Kim, J. U.; Kim, S. O. *ACS Nano* **2013**, *7*, 8899−8907.
(50) Shin, D. O.; Lee, D. H.; Moon, H.-S.; Jeong, S.-J.; Kim, J. Y.; Mun, J. H.; Cho, H.; Park, S.; Kim, S. O. *Adv. Funct. Mater.* **2011**, *21*, 250−254.